Hanger Intersection Points in Box Sections of Steel Bridges Chords – Calculation Models for Consistent Dimensioning Rules

Francesco Aigner[1] *& Josef Fink*[2]

Keywords: arched bridges; hanger intersection; detailing; modelling; FEMresearch; fatigue.

Abstracts: An optimal solution of the hanger intersection zone in steel bridges with a suspended deck must consider the overall load application of the hanger forces into the deck. For an economic and safe design of the considered detail, the local forces to be transferred by welds must be evaluated carefully. The occurring stresses strongly depend on the occurring stiffness distribution. Based on FEM-research, simple rules for the calculation of these forces are derived for a band width which comprises a great range of reasonable dimension ratios.

1. Contents and goals of the investigation

The presented investigation was performed in interaction with the design of a composite railway bridge which was opened for traffic at the end of March 2013. Fig. 1 shows the main components and the overall dimensions of the bridge according to [ÖBB 2010]:

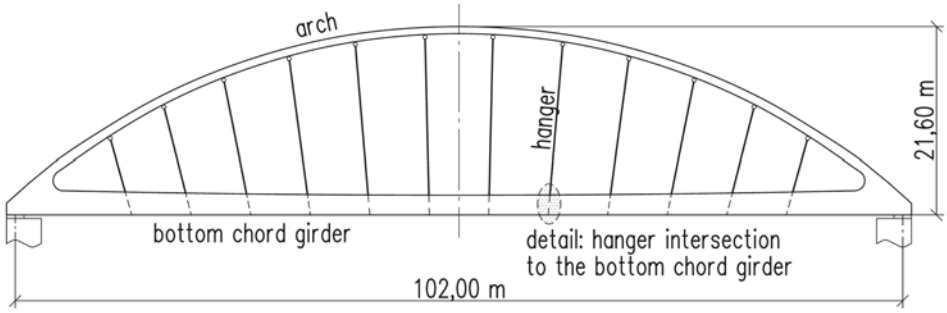

Figure 1: Schematic view of St. Margrethen Rhine Bridge

1 Dipl.Ing. Dr.techn., Vienna University of Technology, Karlsplatz 13, Austria – 1040 Vienna, francesco.aigner@tuwien.ac.at
2 Univ.Prof. Dipl.Ing. Dr.techn., Vienna University of Technology, Karlsplatz 13, Austria – 1040 Vienna, josef.fink@tuwien.ac.at

E. Petzek, R. Băncilă (Eds.), *The Eight International Conference "Bridges in Danube Basin",*
DOI 10.1007/978-3-658-03714-7_13,

The goal of the investigation is the provision of models, formulae and charts for an economic and safe design. In detail, the following items are worked out:

- definition of static models for the derivation of simplified safe though realistic stress regimes both for the dimensioning and verification of the involved components (plates and welds);
- development of verification charts for the components of the intersection;
- computation of design equations for plates and welds, based on the mentioned static models.

These items are realised by means of extensive parameter studies using the FEM [Hauer 2011]. To avoid an inadequate calculating effort, some simplifications concerning the intersection geometry are made. Elastic material behaviour is assumed for all calculations.

Destructive and nondestructive experimental methods are discussed briefly as alternative methods to FEMcalculations.

2. General aspects

Among arch bridge systems with a suspended deck, we have arched bridges with nonoverlapping and with lattice-mode overlapping hangers. In these systems there are hanger intersection points where concentrated loads are introduced into the main girder bottom chords. The magnitudes of the introduced load depend on the dimension of the bridge, on the type of service, and on the number and geometric adjustment of the hangers.

While ULS verifications may be performed on simplified models considering the equilibrium conditions but disregarding compatibility conditions, stress verifications in the serviceability limit state (SLS) and fatigue limit state (FLS) must also allow for the compatibility. The following verifications are to be performed:

- Verifications in the ultimate limit state (ULS), comprising resistance verifications of crosssections and buckling resistance verifications of members. Provided local buckling cannot occur, plastic stress distribution may be allowed for;
- Verifications in the serviceability limit state (SLS). Besides deformation verifications, it must be proven that the occurring stresses remain below the yield strength. Here, the stress regime must be determined for elastic material behaviour, with selfequilibrating residual stresses being neglected;
- Verifications in the fatigue limit state (FLS). Here, again, the stress regime is determined for elastic material behaviour. Residual stresses are allowed for either by using the proper detail category according to [EN 199319 2013], Tab. 8, or by an alternative method as defined in [EN 199319 2013].

Additional or alternative investigation methods to the numeric simulation comprise strain and / or deflection monitoring as well as destructive laboratory tests performed to detect crack initiation sites and to quantify the fatigue resistance. Laboratory tests can be performed on original scale specimens for a comprehensive understanding of the fatigue behaviour, for an optimizing of some geometrical parameters (cope holes, shovelshaped junctionelement, plate thickness ratios) and to verify the results of FEManalyses. However,

original scale fatigue tests consume huge amounts of testing, economic and time resources and do not allow observing in detail the inside of the box section.

3. The investigated hanger intersection detail – execution, idealization and modelling

3.1 Dimensions and investigated parameter ranges

The investigated hanger intersection detail comprises a cutout of the truss chord and the intersection detail itself, consisting of a shovelshaped forging welded on a connecting plate which for its part is welded the top flange of the chord, and the diaphragm which shall absorb the major part of the hanger force. To allow perfect welding, cope holes are provided wherever needed. The most interesting cope holes are the ones at the upper corners of the diaphragm. The radii of these holes depend directly on the width of the intersection shovel and are designed to avoid notching as far as possible.

The detail asbuilt, however, presents a series of arbitrary parameters which not only vary from bridge to bridge but can also vary within one bridge. For a general investigation and to get general, nonspecific results the geometry is simplified, though saving the characteristic properties. A vertical section of the simplified geometry is shown in fig. 2 (left and middle frame).

To avoid too large structures to be computed, the truss chords lengths are limited to a value to attain a uniform stress regime as defined in Bernoulli's hypothesis. According to St. Venant's principle, the self-balancing stress regime occurring at the intersection area itself does not affect but a fairly restrained area. Therefore a section comprising a short length of the hanger, the shovel and the connecting plate, the diaphragm, and adjacent parts of the box section chord, and omitting all ineffectual parts of the construction suffices. A further, very effective simplification concerns the angles which are uniformly set to 90° between all involved plates. The simplified section with full notation is shown in the left and middle frame of fig. 2. The chosen mechanic model to be analysed by FEMsimulations comprises all details to be analysed. It guarantees a sufficient accuracy in the results, yields simple though consistent formulae for verification and is adaptable to a great band of eligible layouts.

The analysed sections and the investigated stresses will be specified in detail in chapter 4.

3.2 Dimensions and investigated parameter ranges

Tab. 1 shows the dimension ranges and ratios on which the parametric study is based. The codenumbers specified in the first column „No." apply to fig. 2.

Table 1: Dimensions for the parametric study

No.	Element	Symbol	Dimensions [mm]	Notes
1	hanger / hanger butt	---	100	invariable
2	shovelshaped junctionelement	---	length: 450	invariable
		---	width: 100 … 410	
		---	thickness: 100 … 40	
3	intersection plate	---	length: 200	invariable
		… L_{AA}	width: 410 … 450	
		---	thickness: 40	
4	box section flange	t_f	35 to 105	---
		(= b_{dia})	(500 to 1000)	
5	box section webs	t_w	18	invariable
		h_w	1500 to 3000	---
6	diaphragm	t_{dia}	40	invariable
		b_{dia}	500 to 1000	---
		L_{BB}	450	invariable
		r	25 to 275	---
		h_{dia}	1500 to 3000	---

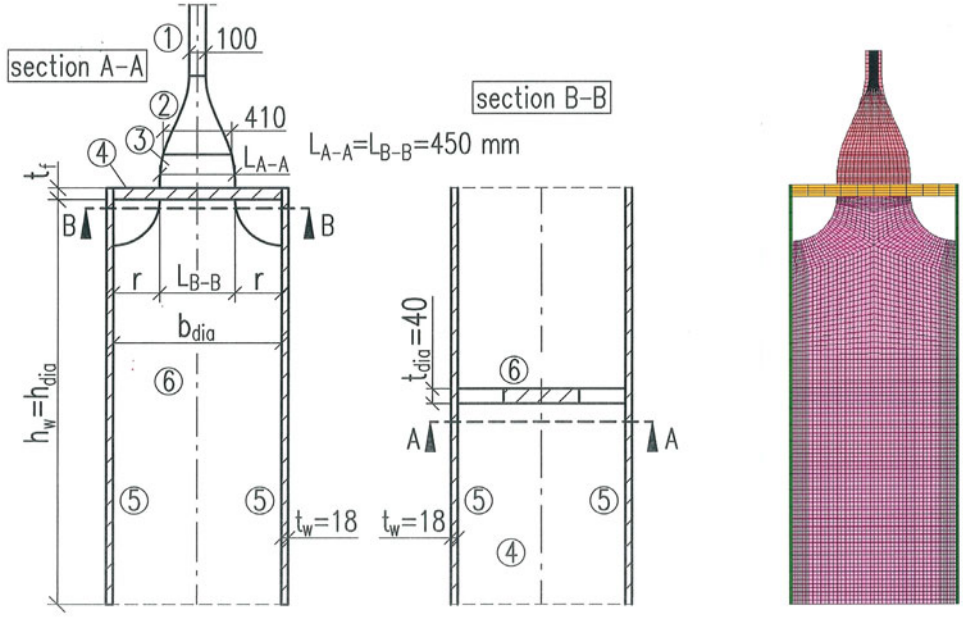

Figure 2: Intersection detail: idealization (left and middle frame) and FE-mesh (right frame from [Hauer 2011])

The considered length ratios are: $0{,}45 \leq \frac{L_{A-A}}{b_{dia}} \leq 0{,}90$ and $1{,}5 \leq \frac{h_{dia}}{b_{dia}} \leq 6{,}0$.

The chosen dimensions and dimension ranges exceed to a significant degree the values as built in the bridge shown in fig. 1, thus enabling the performed results of FEM-analyses to be used for a great range of ordinary applications.

4. The examined sections

Fig. 3 shows the examined sections, the results of which can become controlling for dimensioning or verifications, and the occurring stress definitions. Therein, the code numbers refer to tab. 1. Sections AA and BB are considered to check the uniformity or to detect nonuniformities in the distribution of direct stress. Additionally, the amount of the hanger force absorbed by the diaphragm and the amount transferred to the box girder webs by bending of the flange are quantified. Section CC is considered to study the shear flow occurring between the box section flange and webs. Section DD, finally, shall reveal the shear flow along the edges of the diaphragm. The shear flows in CC and DD serve for the dimensioning of the welds.

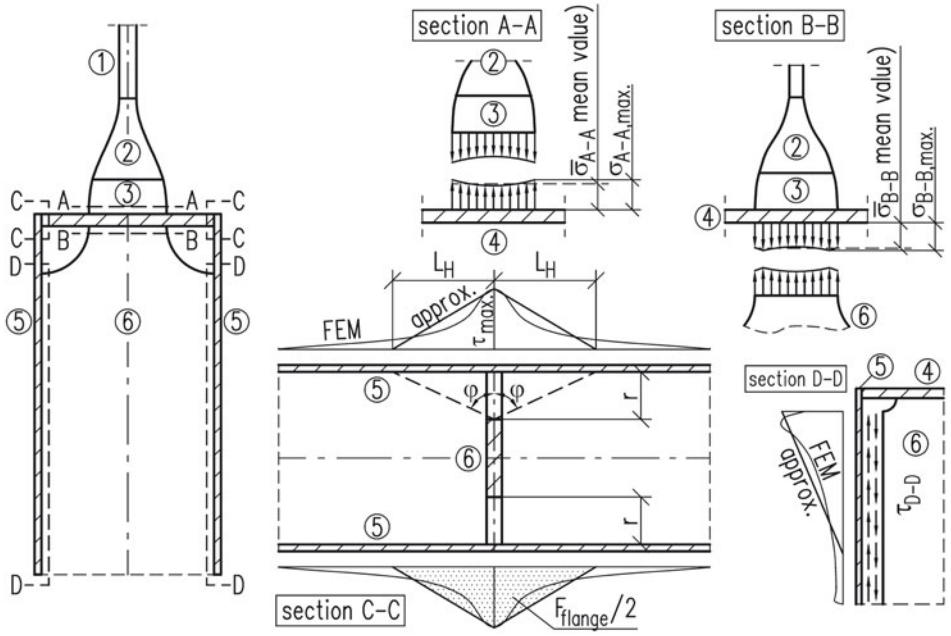

Figure 3: Examined sections and stress definitions

5. FE-program and FE-modelling

5.1 Computer program, preprocessing and postprocessing

As an individual adaptability of the meshing was desired for the present scientific application, the software package „MARC MENTAT 2010" [Marc 2010] was used. Therein, the preprocessor requires manual meshing including the nodal coordinates, the connectivities,

the element types and the boundary conditions. As usual, fine meshing was performed in the investigated, sensitive area of the FEmodel, while wider meshing was done in the areas off these ones. The basic length was taken to 25 mm. Lesser lengths derived from the basic value were taken to model the regions directly nearby the investigated, critical sections. In this way the number of unknowns could be limited to a reasonable number. A vertical section of the FEmesh nearby the diaphragm is shown in fig. 2 (right frame).

Compared to automatic meshing, manual meshing requires some additional effort. This effort, however, is compensated through a variable, problem-related meshing and element choice, and allows avoiding sections running through the elements or skew sections in post-processing.

5.2 Element types

Due to fine meshing in the investigated regions, simple eightnodal volume elements with second order basis functions proved to be sufficient. For details concerning an optimal element and meshing application, reference is made to [Hauer 2011] (p. 11 f.) and to Marc Mentat 2010 product documentation [Marc 2010].

5.3 Model requirements

To save computing time, the overall dimensions of the static model were taken as small as possible. A model which is capable to characterise the stress regime in the investigated hanger intersection area shall fulfil the following requirements:

- the stress regime in the investigated intersection area shall not depend on the chord length, i.e. the chord length shall not interfere with the stress regime itself;
- the distribution of axial and shear stresses at the model ends shall match the distribution according to the elementary Euler-Bernoulli beam theory.

A series of preliminary calculations yielded the model shown in fig. 4. The load introducing lengths at the bottom lines of the web are 3000 mm per web and per side. The code numbers refer to tab. 1.

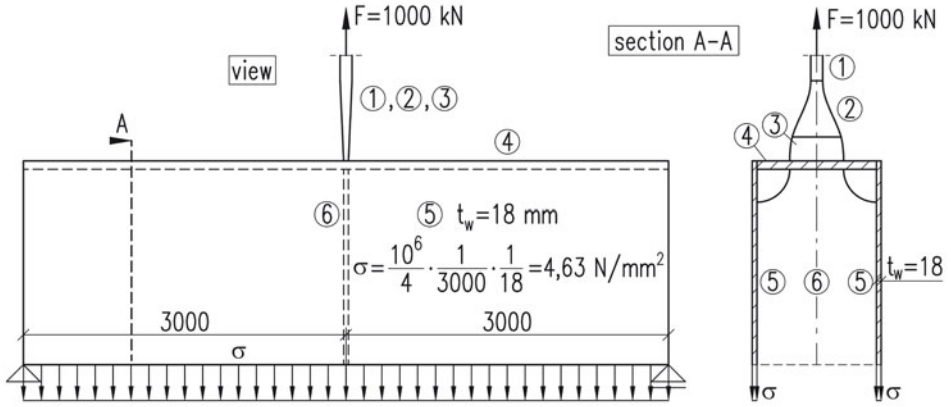

Figure 4: Optimised model for numerical analysis

6. Design charts and formulae

The results of FEMcalculations are summarised in design charts and formulae which will be presented in 6.1. to 6.5.

6.1 Normal stresses in section AA

In section AA, the full hanger load F is introduced into the box section. While a uniform strain could be assumed for ULS-verifications, a more accurate stress analysis is required for SLS und FLS verifications. Within a length of about at both ends of the section the stress increases to the maximum values which are reached at the ends. The increase depends on the flange thickness t_f and on the ratio . The normal stresses as results from FEManalyses for t_f = 35 mm and series of values (and, thus, of radii r) are shown in fig. 5. Therein, the code numbers refer to tab. 1.

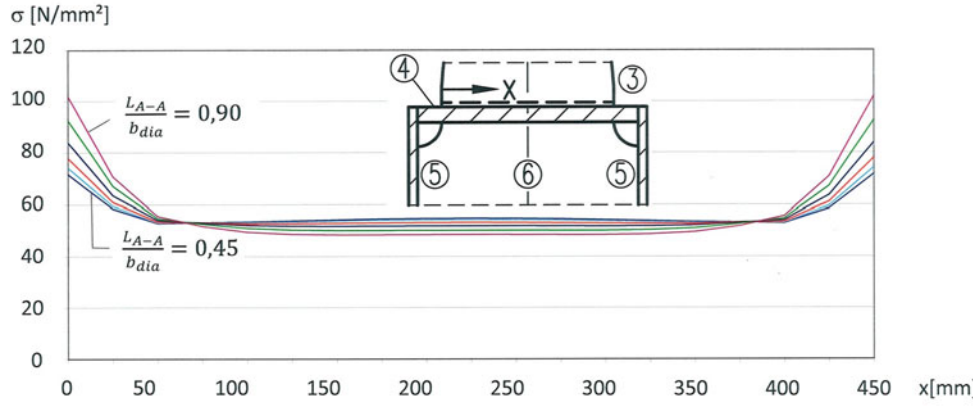

Figure 5: Normal stress distribution in section AA (from [Hauer 2011])

The complete design chart comprises the results of FEManalyses given in fig. 6, as well as a simple approach for practical use.

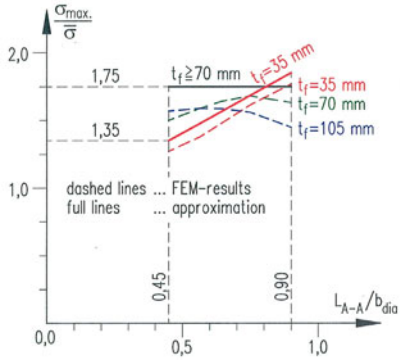

The analytical approach reads:

$$\frac{\sigma_{max.}}{\bar{\sigma}} = \frac{L_{A-A}}{0{,}9 \cdot b_{dia}} + 0{,}85$$

for $t_f = 35\ mm$ and $0{,}45 \leq \frac{L_{A-A}}{b_{dia}} \leq 0{,}90$ and

$$\frac{\sigma_{max.}}{\bar{\sigma}} = 1{,}75$$

for $t_f \geq 70\ mm$ and $0{,}45 \leq \frac{L_{A-A}}{b_{dia}} \leq 0{,}90$

Figure 6: Increase factors

6.2 *The Factor f*

Depending on the flange thickness t_f and on the size r of the cut holes related to the further remaining lengths, varying parts of the hanger force F are absorbed by the diaphragm, , or transferred to the chord webs of the box section by bending of the flange: . The values are shown in fig. 7 as well as the rule itself. The complete design chart comprises the results of FEManalyses and a practical approach.

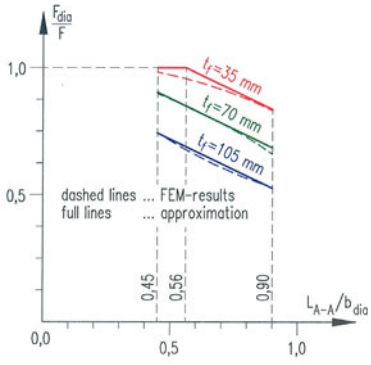

The analytical approach reads:

$$f = \frac{F_{dia}}{F} = d - 0{,}482 \cdot \frac{L_{A-A}}{b_{dia}} \text{ but } f \leq 1{,}0. \text{ Herein:}$$

$$d = 1{,}27 \text{ for } t_f = 35\ mm \text{ and } 0{,}45 \leq \frac{L_{A-A}}{b_{dia}} \leq 0{,}90$$

$$d = 1{,}12 \text{ for } t_f = 70\ mm \text{ and } 0{,}45 \leq \frac{L_{A-A}}{b_{dia}} \leq 0{,}90$$

$$d = 0{,}96 \text{ for } t_f = 105\ mm \text{ and } 0{,}56 \leq \frac{L_{A-A}}{b_{dia}} \leq 0{,}90$$

Anyway, $f \leq 1{,}0$

Figure 7: Force ratio

6.3 *Normal stresses in section BB*

In section BB, the portion f · F of the hanger load F is introduced into the diaphragm stiffening the boxshaped girder. While a uniform strain of f · F or even of F (then neglecting flange bending and shear) might be sufficient for ULS-verifications, a more accurate stress analysis

must be performed for SLS und FLS verifications. Fig. 8 shows that controlling maximum values exceeding the mean values occur at some distance from the ends. The ratios of the maximum values and the mean values depend on the flange thickness t_f and on the ratio L_{BB} / b_{dia}. The results for $t_f = 35$ mm and series of values (and, thus, of radii r) are shown in fig. 8. Therein, the code numbers refer to tab. 1.

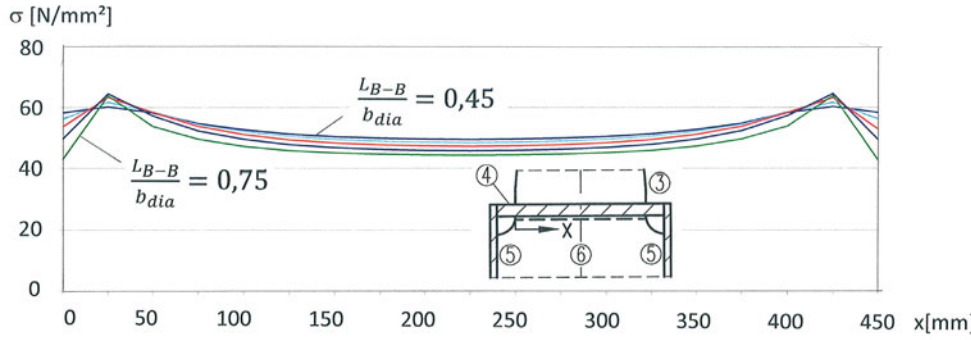

Figure 8: Normal stress distribution in section BB (from [Hauer 2011])

The complete design chart comprising the results of FEManalyses and a practical approach are given in fig. 9.

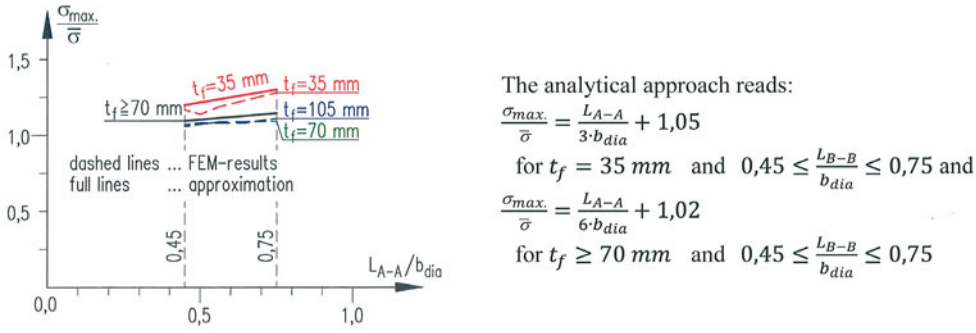

Figure 9: Increase factors

6.4 Shear stresses in section CC

As stated in 6.2., a part of the total hanger force F is being introduced into the diaphragm, while another part is transferred by plate bending of the box girder flange to the welds in sections CC. The distribution of vertical shear shown in fig. 10 is controlling for the local dimensioning of the longitudinal welds. Fig. 10 applies for $t_f = 105$ mm. It is mentioned that the shear stresses given in figure 10 refer to the total hanger force F. (The sum of the forces introduced into the webs of the girder is necessarily smaller than the hanger force F itself.)

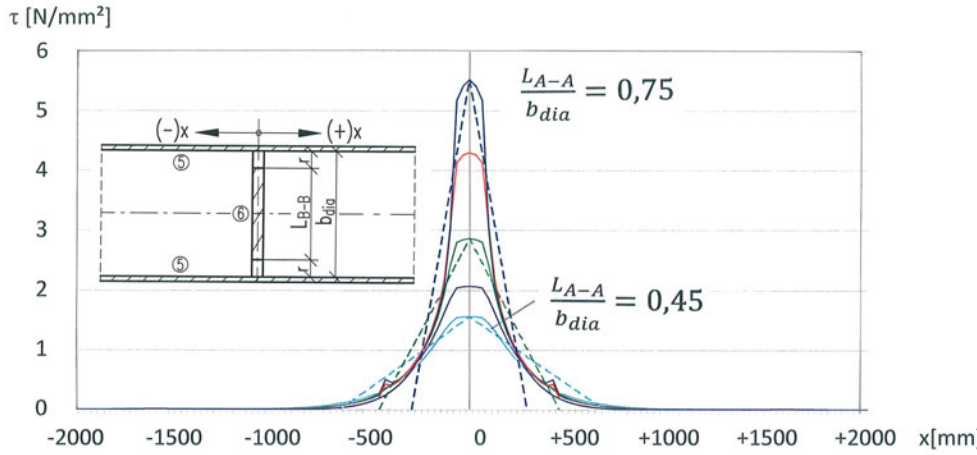

Figure 10: Shear stress distribution in section CC (from [Hauer 2011])

In contrast to the values analysed in 6.1., 6.2., 6.3. and 6.5., an effective simplification is not easy to find here. At best, the angle as defined in fig. 3 is expressed in dependency on . The graphs are given in fig. 11.

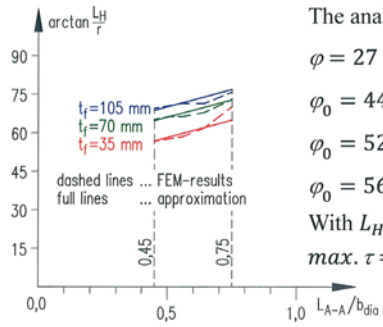

The analytical approach reads:

$$\varphi = 27 \cdot \frac{b_{B\text{-}B}}{b_{dia}} + \varphi_0\ [deg]\ \text{Herein,}$$

$$\varphi_0 = 44{,}6\ [deg] \quad \text{for} \quad t_f = 35\ mm \quad \text{and} \quad 0{,}45 \leq \frac{L_{B-B}}{b_{dia}} \leq 0{,}75$$

$$\varphi_0 = 52{,}6\ [deg] \quad \text{for} \quad t_f = 70\ mm \quad \text{and} \quad 0{,}45 \leq \frac{L_{B-B}}{b_{dia}} \leq 0{,}75$$

$$\varphi_0 = 56{,}6\ [deg] \quad \text{for} \quad t_f = 105\ mm \quad \text{and} \quad 0{,}45 \leq \frac{L_{B-B}}{b_{dia}} \leq 0{,}75$$

With $L_H = r \cdot tan\varphi$ we get the expression for the maximum shear stress:

$$max.\ \tau = \frac{(1{,}05-f)\cdot F}{2} \cdot \frac{1}{r \cdot t_f \cdot tan\varphi}$$

Figure 11: Angles ϕ depending on parameter

6.5 Shear stresses in section DD

The part f · F of the total hanger force F which is introduced into the diaphragm is diverted to the webs of the box girder section. Fig. 12 shows the shear stresses in the webs as results of FEManalyses (continuous lines) and approximations (dashed lines) for t_f = 35 mm.

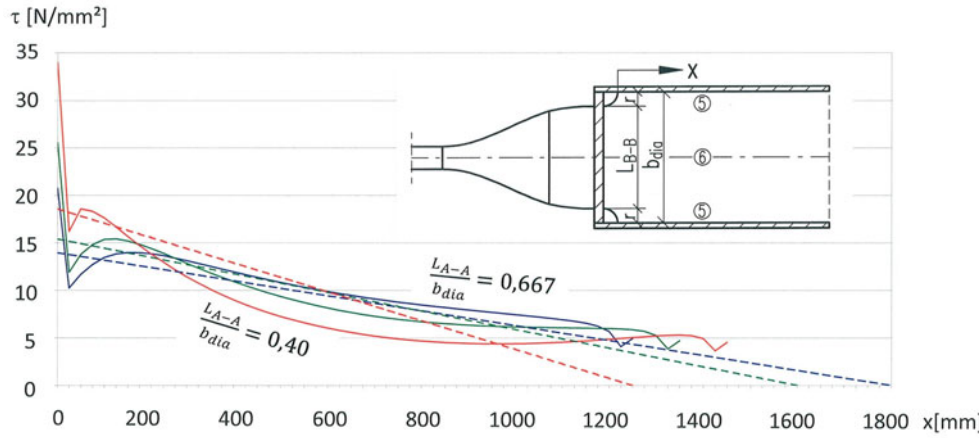

Figure 12: Shear stress distribution in section DD (from [Hauer 2011])

Depending on the ratio between the diaphragm width and height, two characteristic shapes of shear-flow can occur, see fig. 13. Therein, the code numbers refer to tab. 1.

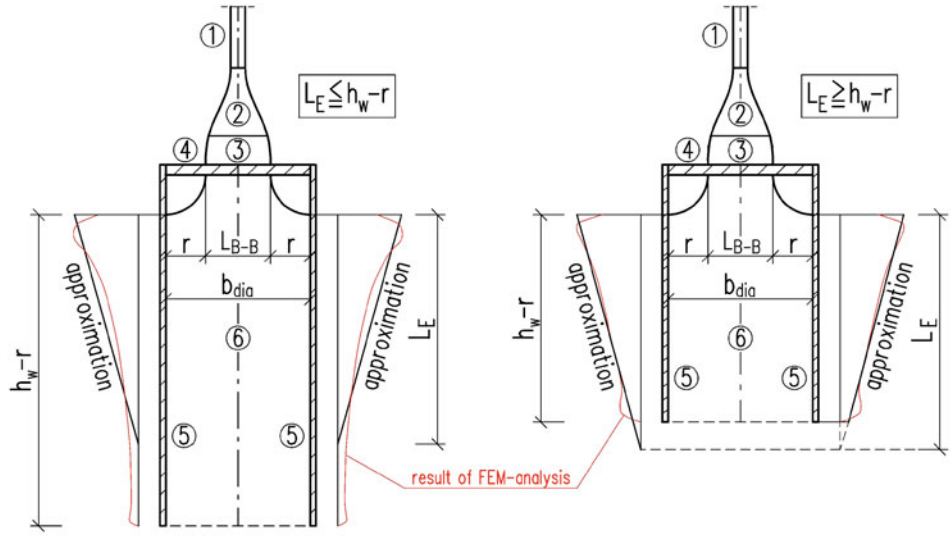

Figure 13: Stress distribution in section DD

The basis values of the triangular or trapezoidal approximate solutions can be defined by means of the ideal length L_E which may result greater or less than the actual weld length $h_w - r$. The diagrams representing the lengths L_E are given in fig. 14.

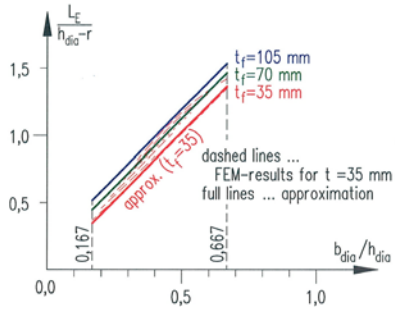

The analytical approach reads:

$$n = \frac{L_E}{h_{dia}-r} = 2{,}03 \cdot \frac{b_{dia}}{h_{dia}} + d \quad \text{Herein,}$$

$$d = 0{,}01 \quad \text{for} \quad t_f = 35\,mm \quad \text{and} \quad 0{,}167 \le \frac{b_{dia}}{h_{dia}} \le 0{,}667$$

$$d = 0{,}11 \quad \text{for} \quad t_f = 70\,mm \quad \text{and} \quad 0{,}167 \le \frac{b_{dia}}{h_{dia}} \le 0{,}667$$

$$d = 0{,}18 \quad \text{for} \quad t_f = 105\,mm \quad \text{and} \quad 0{,}167 \le \frac{b_{dia}}{h_{dia}} \le 0{,}667$$

The maximum shear stress in the webs amounts to

$$max.(\tau \cdot t_{dia}) = \frac{f \cdot F}{L_E}, \text{ wherein}$$

$$L_E = n \cdot (h_{dia} - r) \text{ (ideal length)}$$

Figure 14: Auxiliary values $n = L_E/(h_{dia} - r)$ for the calculation of L_E and of the maximum shear.

7. Weld types

Besides the static need the checkability of the ready-made welds is a controlling item concerning the execution. Perfect check of the entire weld is necessary for the highly stressed welds in sections AA and BB and can be guaranteed only by full penetration doublebevel groove welds. As full welding is de facto unfeasible the welds in sections CC and DD and remarkable stress gradients occur (the maximum stresses are restrained just within small areas of pronounced peaks), singlebevel groove welds are realised in sections CC and double fillet welds in sections in sections DD. The chosen weld types are shown in fig. 15, wherein, the code numbers refer to tab. 1.

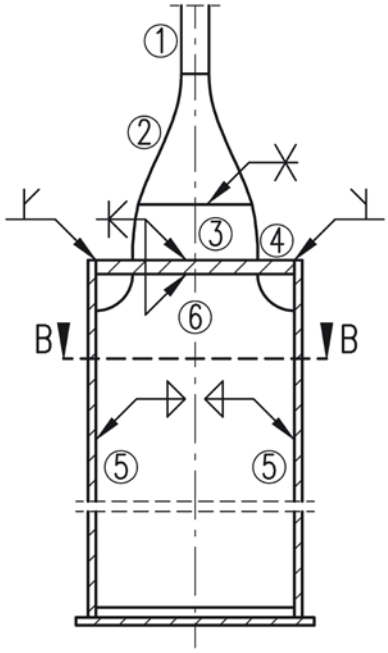

Figure 15: Weld types

8. Summary and outlook

To quantify the stress regime and the dimensions of welds occurring in a standard hanger intersection detail of a bridge deck, parametric studies based on FEMcalculations were performed. The effects of individual geometrical data were analysed in detail, and the results of the investigations were summarised in design charts. Recommendations for an economic and safe weld disposition are given.

Further investigations should include:

- Allowance for other than the investigated thicknesses of the diaphragm (taken to 40 mm here) and of the webs (taken to 18 mm here);
- Optimising of the geometrical shape of the shovelshaped junctionelements and of the joint plates to mitigate the stress peaks at the ends, occurring especially in combinations with thinner flange plates.

References

[ÖBB 2010] ÖBB (Austrian Federal Railways): Stahlbaupläne des Ausführungsprojektes „Umbau St. Margrethen (CH) – Lustenau (A) Rheinbrücke“ 2010.

[Hauer 2011] Hauer, B.: Herleitung von Rechenmodellen zur Spannungsberechnung für ein Hängeranschluss-Detail einer Stabbogenbrücke auf Basis von Parameterstudien. Master Thesis, TU Wien 2011.

[EN 199319 2013] Eurocode 3: Design of steel structures - Part 1-9: Fatigue.

[Marc 2010]: „Marc Mentat 2010”, product documentation. Element library.